Mathematical modeling of tumor growth and treatment

Heiko Enderling[1,2,*], Mark A.J. Chaplain[3]

[1]Center of Cancer Systems Biology, St. Elizabeth's Medical Center, Tufts University School of Medicine, Boston MA, USA

[2]new address: Integrated Mathematical Oncology, H. Lee Moffitt Cancer Center and Research Institute, Tampa, FL, USA

[3]Division of Mathematics, University of Dundee, Dundee, Scotland, UK

[*]Correspondence:

Heiko Enderling

Integrated Mathematical Oncology

H. Lee Moffitt Cancer Center and Research Institute

12902 Magnolia Drive Tampa, FL 33612

Tel: (813) 745 - 4316

Fax: (813) 745 – 6497

Email: heiko.enderling@moffitt.org

Abstract

Using mathematical models to simulate dynamic biological processes has a long history. Over the past couple of decades or so, quantitative approaches have also made their way into cancer research. An increasing number of mathematical, physical, computational and engineering techniques have been applied to various aspects of tumor growth, with the ultimate goal of understanding the response of the cancer population to clinical intervention. So-called *in silico* trials that predict patient-specific response to various dose schedules or treatment combinations and sequencing are on the way to becoming an invaluable tool to optimize patient care. Herein we describe fundamentals of mathematical modeling of tumor growth and tumor-host interactions, and summarize some of the seminal and most prominent approaches.

Keywords: ordinary differential equation, partial differential equation, tumor modeling, angiogenesis

Introduction

Mathematical modeling is a powerful tool to test hypotheses, confirm experiments, and simulate the dynamics of complex systems. In addition to helping understand the mechanistic underpinnings of dynamical systems, mathematical models simulate complex systems in a relatively fast time without the enormous costs of laboratory experiments and the corresponding biological variations. In particular for oncology, such models can be calibrated using experimental or clinical data [1-3], and competing hypotheses of tumor progression can be evaluated and treatment options thoroughly analyzed before clinical intervention [4-8]. Techniques for quantitative modeling are plentiful, and an increasing number of theoretical approaches are successfully applied to cancer biology. Differential equation models and individual-based cell models paved the way into quantitative cancer biology about two decades ago. Herein we will give an introduction on how such models are derived and how they can be utilized to simulate tumor growth and treatment response. We will then discuss a number of different models and discuss their confirmative and predictive power for cancer biology.

Ordinary differential equation models of tumor growth

The number of cancer cells in a tumor is difficult to estimate due to constant changes in time. Tumor cells may proliferate, rest in a quiescent state, or die. Describing the number of tumor cells as a function of time is therefore remarkably challenging. It is, however, straightforward to formalize what changes in cell number are expected as time changes. The number of living cells only changes when cells proliferate or die:

difference in *live* cell number over time interval = number of cells *created* and *died* over time interval

How many and how often cells proliferate and how many cells die is dependent on the considered time difference, i.e., *dt* (where *d* stands for difference and *t* stands for time). Let us assume the cell cycle length of an arbitrary cancer cell is 24 hours. Then, over the course of one day, the probability that the cell divides is close to 100%. Without knowing at what position in the cell cycle a cell currently is, we can assume that the probability of this cell to divide within the time frame of one hour is 1/24. Not knowing the exact number of cells in a tumor population, the above example can be directly translated to the population level. For a population of unsynchronized cells with a cell cycle length of 24 hours we can assume that all cells divide once if *dt*=24 hrs. Similarly, if *dt*=1hr, only a fraction of cells in the population (about 1/24) is expected to divide. One reasons similarly for cell death. We therefore must introduce the time difference as well as two parameters into the above equation:

$$\frac{\text{difference in number of cells}}{dt} = +a \text{ (number of cellls)} \quad - b \text{ (number of cells)},$$

where α and β are respectively understood as the fraction of dividing and dying cells each *dt,* and hence denote the per capita growth and death rates of the total cell population. It is obvious that the cell number must increase after a proliferative event and decrease after a cell death event. Let us introduce variable *c* as number of cells. The difference in cell number then becomes *dc*, and the above equation can be written as:

$$\frac{dc}{dt} = \alpha c - \beta c. \qquad (1)$$

Such equation is called an ordinary differential equation (ODE).

Let us assume that at time *t*=0, i.e., the starting point of an experiment, we have one million cells, i.e. $c=10^6$. Population growth dynamics can follow one of three fates: (i) if

$\alpha = \beta$, then $dc/dt = 0$. In this case the number of cells in the population does not change and the population exhibits a state of tumor dormancy. It is of note that either $\alpha = \beta = 0$, that is all cells in the population are in state of cellular dormancy or quiescence, or $\alpha = \beta > 0$ in which case cell proliferation is balanced by cell death [9,10]. If (ii) $\alpha > \beta$, then $dc/dt > 0$ and the cell population will continuously grow with greater α-β rates yielding faster growth. On the other hand, the population will monotonically decrease if (iii) $\alpha < \beta$ and thus $dc/dt < 0$ (figure 1).

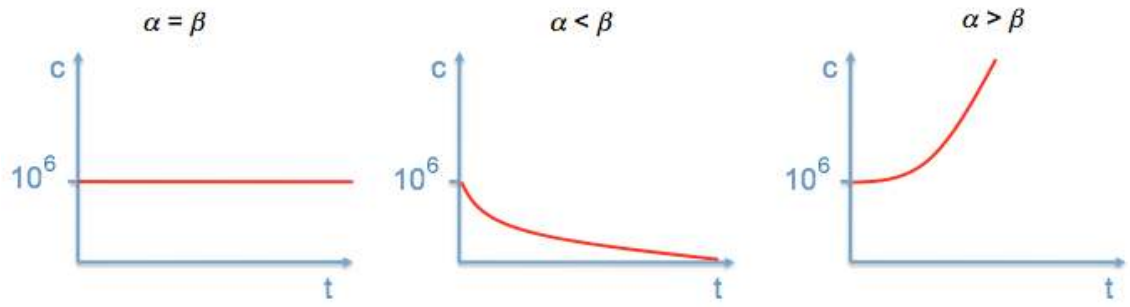

Figure 1. Growth dynamics of cell population c over time t for different relative rates of cell proliferation α and cell death β; $c = 10^6$ cells at time t=0.

Eqn. (1) can be reduced to a one-parameter problem. The terms αc-βc can be combined into the single term $(\alpha$-$\beta)c$, and we introduce the single parameter, λ, λ=α-β, which is called the net population growth rate. The differential equation describing cell population change over time is then

$$\frac{dc}{dt} = \lambda c. \qquad (2)$$

As before, if $\lambda<0$, $\lambda=0$, or $\lambda>0$ the population decreases, remains at a constant size, or increases respectively. Experimental data from *in vitro* or *in vivo* population studies can then be used to parameterize such model (figure 2).

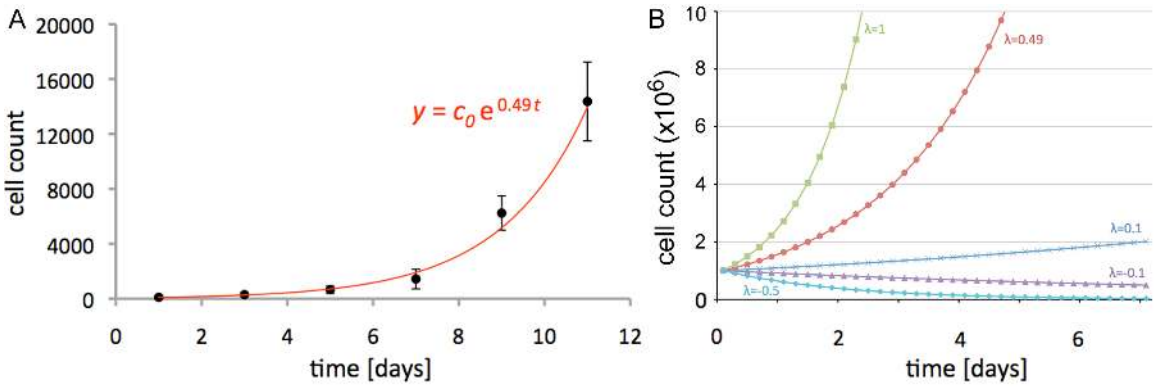

Figure 2. A) Mock population growth comparable to *in vitro* experimental data with 5% standard error bars (black dots) and calculated trend line (red). **B)** Mathematical model results of population growth for different parameters of λ.

Dynamic tumor growth rates

Defining a constant per capita growth rate to model tumor growth yields exponentially growing cell populations and neglects carrying capacity constraints. Solid tumors initially grow rapidly, but growth decelerates as tumors grow bigger [11-14]. Therefore, the per capita rate of tumor growth should depend on the tumor size c and not remain constant [15]

$$\frac{dc}{dt} = f(c) \cdot c .$$

A classic example of a per capita rate of tumor growth dependent on tumor size relative to the host carrying capacity K is given by the logistic model [16]

$$\frac{dc}{dt} = \lambda c\left(\frac{K-c}{K}\right) \quad = \quad \lambda c\left(1-\frac{c}{K}\right). \qquad (3)$$

Here, $f(c) = \lambda\left(1-\frac{c}{K}\right)$, and thus the per capita growth rate decreases as c increases. If tumor volume, or population size $c << K$, then $\left(1-\frac{c}{K}\right) \approx 1$ and growth is approximately exponential as is yielded by eqn. (2) above. As the population grows and approaches the carrying capacity K, however, $\left(1-\frac{c}{K}\right) \to 0$ and population growth is impeded. Figure 3 shows the evolution of population size as well as the growth rate dependent on population size relative to K for different parameters λ.

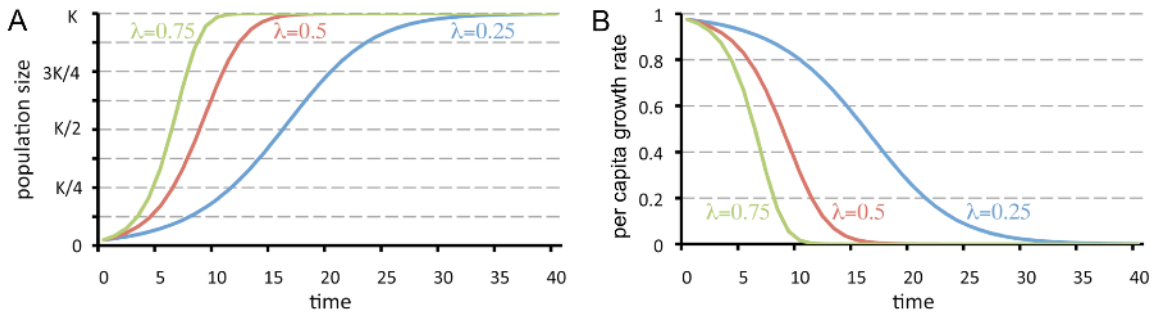

Figure 3. Population growth limited by carrying capacity *K*. A) Population size as a function of time using eqn. (2). **B)** Corresponding dynamic per capita growth rates.

Numerous dynamic growth rate functions with applicability to tumor growth have been discussed [14,15]. The so-called Gompertz curve [17] has been shown to be applicable to biological growth that decelerates with population size [18], and therefore

to observed tumor growth slowdown with tumor size [11,12,19,20]. The growth rate is the negative logarithm of the current population size divided by the carrying capacity:

$$\frac{dc}{dt} = -\lambda c \log\left(\frac{c}{K}\right). \qquad (4)$$

Despite a more rapid growth rate fall-off, population growth mimics that observed with eqn. (3) and given in figures 3 (fig. 4).

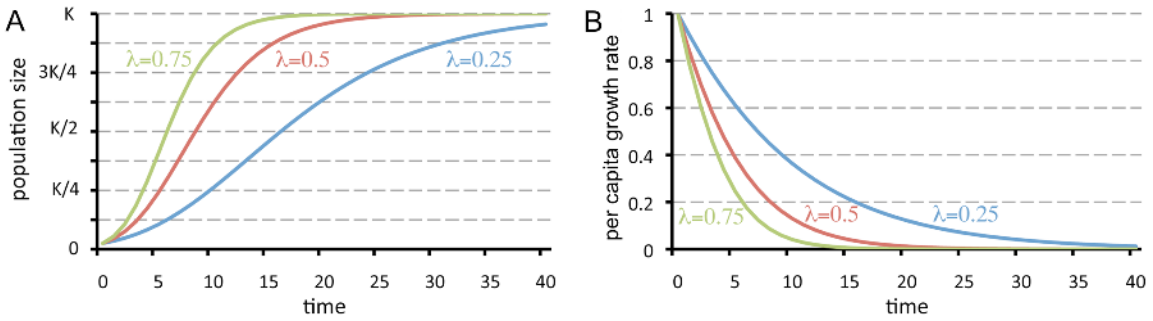

Figure 4. Gompertz population growth limited by carrying capacity *K*. A) Population size as a function of time using eqn. (4). **B)** Corresponding dynamic per capita growth rates.

In a pathological setting, the carrying capacity itself can be non-constant. Increase in cell mass and physical pressure may yield deformation and expansion of basement membranes thereby increasing the spatial carrying capacity dependent on tumor size. Tumor growth, however, can also stall in absence of necessary growth factors and nutrients provided by the host vasculature. During vascular dormancy the diffusion of oxygen and nutrients into the tumor interior is limited resulting in a balance of cell proliferation and cell death [9]. The carrying capacity then defines the maximum tumor size that can be supported by vascular supply. Through release of pro- and anti-

angiogenic factors the tumor population interacts with the host vasculature thus giving a carrying capacity K that changes in time. Through diffusion-consumption arguments Hahnfeldt and colleagues derived that vasculature inhibition is relative to the (tumor volume)$^{2/3}$ [21]. Instead of being constant, changes in K are expressed by $\frac{dK}{dt}$:

$$\frac{dK}{dt} = \overbrace{\phi c}^{\text{stimulationary capacity of the tumor upon inducable vasculature}} - \overbrace{\varphi K c^{2/3}}^{\text{endogenous inhibtion of previously generated vasculature}}, \quad (5)$$

where ϕ and φ are constant positive rates of angiogenesis stimulation and inhibition, respectively. Initially tumor growth is accelerated due to abundant stimulation but as the tumor grows the inhibitory effects will outweigh the stimulator yielding a plateau vascular supply and tumor size (fig. 5).

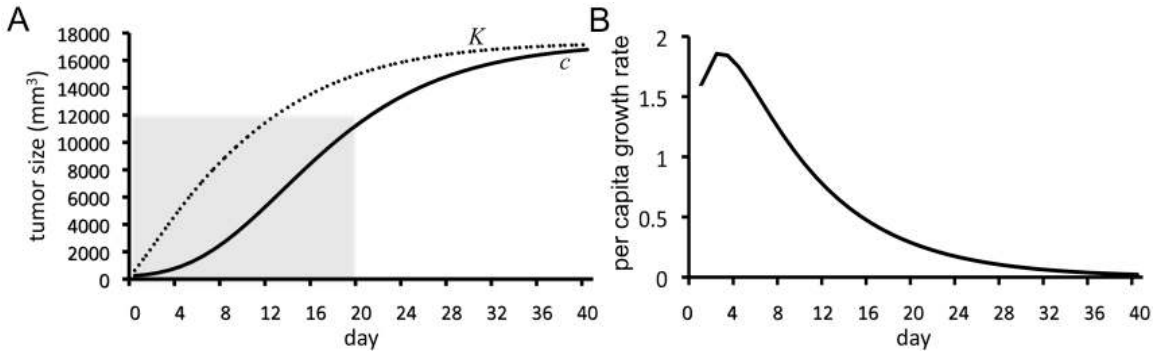

Figure 5. Tumor evolution with a dynamic carrying capacity. A) Evolution of tumor size c (solid plot) and carrying capacity K (dotted) with λ=0.192, ϕ=5.85, and φ=0.00873, parameters fitted to Lewis lung carcinoma growing in C57BL/6 mice in Hahnfeldt et al. [21] (the shaded area corresponds to the plot reported in that paper). **B)** Corresponding dynamic per capita growth rates.

Modeling tumor treatment

Tumor treatment can follow two different strategies. A gross reduction in tumor volume can be inflicted by inducing cell death in proliferating cancer cells, or by decreasing the tumor support via reduction of carrying capacity. The effects of both forms of cancer treatment can be readily included in differential equation models. Let us consider the modified Hahnfeldt model [21] (eqns. (4) & (5)):

$$\frac{dc}{dt} = -\lambda c \log\left(\frac{c}{K}\right) - \overbrace{\xi c}^{\text{anti-tumor treatment}}$$

$$\frac{dK}{dt} = \phi c - \varphi K c^{2/3} - \overbrace{\upsilon K g(t)}^{\text{anti-angiogenic treatment}} .$$

In the simplest case, anti-tumor treatment induces a continuous tumor cell kill with strength $0 \leq \xi \leq 1$, conceivable as chemotherapy or immunotherapy. Figure 6 shows the response of the tumor to such cell kill with different strengths after the tumor has grown for 40 days (c.f. Figure 5). Hahnfeldt and colleagues [21] modeled the inhibition of angiogenesis due to administered anti-angiogenic agents to be proportional to the concentration of the drug *g(t)*, which includes partially cleared drug concentrations from previous administrations

$$g(t) = \int_0^t a(t') \exp\left(-clr(t - t')\right) dt' ,$$

where *a(t')* and *clr(t-t')* are the rates at which the inhibitor concentration is administered and its clearance rate, respectively. Figure 7 shows two different simulations of anti-angiogenic treatments with TNP-470 and Endostatin and a remarkable good fit with experimental data for the chosen parameter sets.

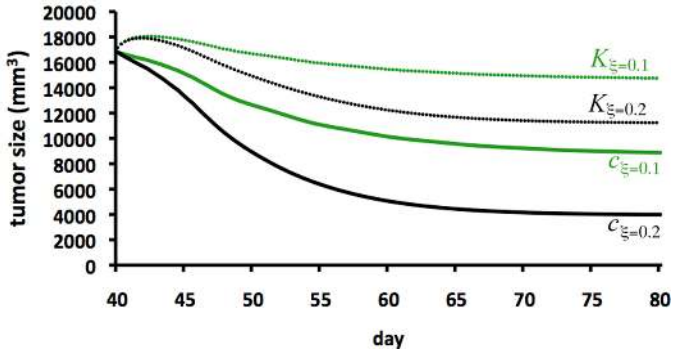

Figure 6. Anti-tumor treatment for different strength cell kill ξ. Anti-tumor treatment continuously applied after day 40 of tumor growth (c.f. figure 5A).

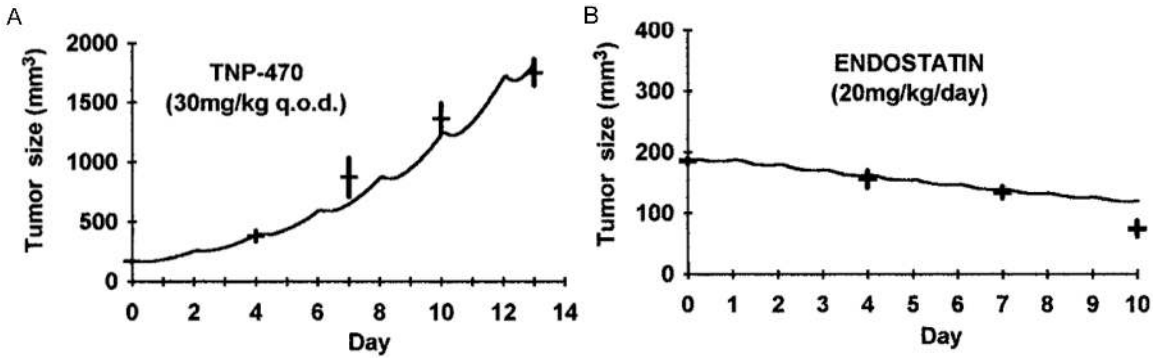

Figure 7. Different anti-angiogenesis treatments applied at the beginning of tumor growth. A) TNP-470, with v=1.3 and clr=10.1 (q.o.d.: every other day). **B)** Endostatin, with v=0.66 and clr=1.7. Continuous curves are model results; horizontal lines with vertical error bars are experimental data. Reproduced from Hahnfeldt et al. [21] (permission pending)

Partial differential equation models of tumor growth

Although ordinary differential equation models have proven to be a useful tool to simulate the evolution of total tumor cell number over time, the most apparent

shortcoming of this approach is the lack of spatial consideration. Patients do not die because of the total number of cancer cells in their body but because the primary tumors locally invade the tissue and spread (metastasize) to distant sites of the body to establish secondary tumors. It is these metastatic masses that are the main cause of death in cancer patients. Cancer invasion and metastatic spread are two crucial and inherently spatial processes, which can be simulated using partial differential equation (PDE) models. In such models, a population n at spatial positions (x), (x,y), or (x,y,z) in one, two, or three-dimensional space, respectively, is often described as a density, or fraction of maximum available volume at this position, and thus scaled between 0%-100%, or 0-1. The variable n is no longer only dependent on changes in time t, but also on variations in considered spatial dimensions. The equation for n therefore involves the partial derivatives of its independent variables. Omitting the considered spatial domain, the partial derivative of n with respect to time t is written as $\frac{\partial n}{\partial t}$.

Invasion of tissue is a key aspect of the growth and spread of cancer and is vital for successful metastasization. The process of invasion consists largely of three components: (i) the cancer cells secrete various matrix degrading enzymes (MDEs); (ii) the MDEs destroy the surrounding tissue or extracellular matrix (ECM); (iii) the cancer cells actively spread into the surrounding tissue through proliferation and migration.

Perhaps the first spatial model of cancer invasion was developed by Gatenby and Gawlinski [22] (inspired by previous work of Gatenby [23]). This model considered the effect of excess H^+ ions in degrading the local tissue, allowing the cancer cells to diffuse

and proliferate into the space created. The system of partial differential equations used to model the spatio-temporal evolution of cancer cells (or neoplastic tissue), c, H^+ ions, m, and extracellular matrix (or normal host tissue), v, is as follows:

$$\frac{\partial c}{\partial t} = \overbrace{\nabla \cdot \left(D_C \left(1-v\right) \nabla c \right)}^{\text{nonlinear diffusion}} + \overbrace{\rho c \left(1-c\right)}^{\text{logistic growth}},$$

$$\frac{\partial m}{\partial t} = \overbrace{\nabla^2 m}^{\text{diffusion}} + \overbrace{\delta \left(c-m\right)}^{\text{production \& decay}},$$

$$\frac{\partial v}{\partial t} = \overbrace{v\left(1-v\right)}^{\text{logistic growth}} - \overbrace{\gamma m v}^{\text{degradation}},$$

where D_c is the (constant) diffusion coefficient, ρ the (constant) cancer cell proliferation rate, δ the (constant) H^+ ions production rate (also taken to be equal to the decay rate) and γ the (constant) extracellular matrix degradation rate. As can be seen from the above equations, the cancer cells proliferate and undergo nonlinear diffusion (dependent on the density of normal tissue – high density of normal tissue giving lower diffusion, low density of normal tissue giving higher diffusion) and secrete H^+ ions, which diffuse and degrade the normal tissue. The H^+ ions also undergo linear decay and the normal tissue is assumed to have logistic growth in order to attain its healthy state in the absence of cancer cells (in the model of Gatenby and Gawlinski, the production and decay of H^+ ions is assumed to have the same rate for algebraic simplicity). For details on the mathematical formulation of diffusion, the population-level description of random cell migration, we refer the interested reader to partial differential equation textbooks. Through a combination of computational simulation and mathematical analysis (travelling wave theory) of the aforementioned system of partial differential equations, Gatenby and Gawlinski predicted the existence of a hypocellular gap at the interface

between the normal and cancerous tissue [22]. This was subsequently observed in hematoxylin-eosin (H&E) stained micrographs of invading cancers (Fig. 8).

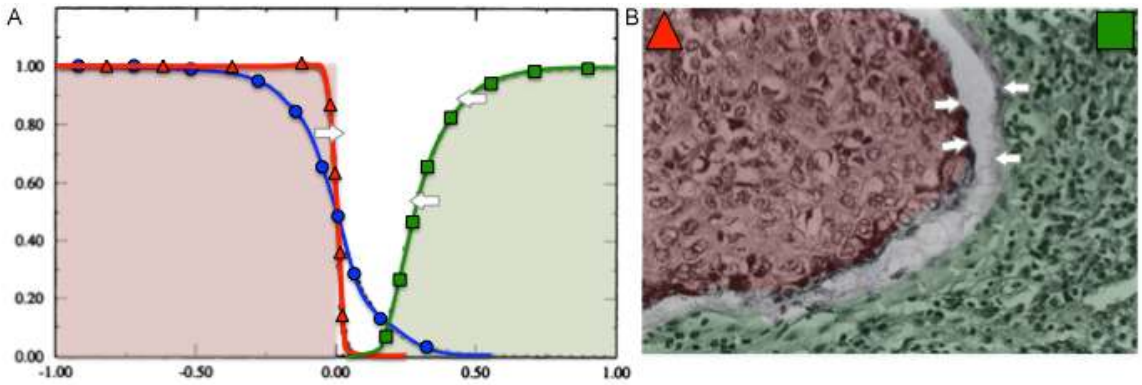

Fig. 8. Simulation results and experimental confirmation of the cancer invasion. A) Computational results. Tumor (red triangles) secretes H^+ ions (blue circles) that diffuse and degrade the extracellular matrix or healthy tissue (green squares). Simulations reveal a gap between the advancing tumor front and the receding tissue (white arrows). **B)** Hematoxylin-eosin (H&E) stained micrograph of the tumor-host interface reveals hypocellular gap (white arrows) as predicted by simulations. Modified from Gatenby & Gawlinski [22] (permission pending)

Subsequent PDE models developed this idea and examined the interplay between cancer cells, c, degrading enzymes, m, and tissue, v, using reaction-diffusion-taxis models, where the process of *haptotaxis* (i.e. directed cell migration in response to gradients of extracellular matrix density or gradients of adhesive molecules in the extracellular matrix) played a key role in the cancer cell migration. The model of Perumpanani et al. [24] was the first to do this. Once again through a combination of computational simulations and travelling wave analysis, predictions were made of the

speed and depth of penetration of cancer cells into the host tissue. The role of haptotaxis was especially studied in the paper of Anderson et al. [25], where a 2-dimensional setting was first used and the influence of the tissue (extracellular matrix) was explicitly explored:

$$\frac{\partial c}{\partial t} = \overbrace{D_c \nabla^2 c}^{\text{diffusion}} - \overbrace{\gamma \nabla \cdot \left(c \nabla v \right)}^{\text{haptotaxis}}$$

$$\frac{\partial m}{\partial t} = \overbrace{\nabla^2 m}^{\text{diffusion}} + \overbrace{\alpha c}^{\text{production}} - \overbrace{\beta m}^{\text{decay}}$$

$$\frac{\partial v}{\partial t} = - \overbrace{\eta m v}^{\text{degradation}} .$$

In this continuum model, cell proliferation was not included in order to focus solely on the role of cancer cell migration in invasion. However, later in that paper {Anderson:2000jf}, cancer cell proliferation was included in the discrete version of the model (see next section). The effect of variable oxygenation and cancer cell adhesion was included in the work of Anderson [26].

Other continuum approaches (i.e. various PDE models) include that of Chaplain and Lolas [27] and Andasari et al. [28] (investigating in more detail the effects of the degrading enzymes, specifically the urokinase plasminogen system), Frieboes et al. [29] (focusing on cell-cell adhesion and a moving boundary approach), and Gerisch and Chaplain [30] and Chaplain et al. [31] (using a continuum model incorporating cell-cell adhesion via a non-local integral term).

Discrete models of tumor growth

In addition to being the first 2-dimensional continuum model of cancer invasion focusing on the role of haptotaxis, the paper of Anderson et al. [25] was also the first to consider a discrete model of cancer cell invasion (now also including proliferation at a discrete level), derived from the continuum PDE model. The computational simulation results of this model explored the observation that individual cancer cells can migrate beyond a "visible margin" of cancerous tissue, which was "detectable" by surgeons. This was perhaps the first paper to explore the issue of stochastic events and probability in invasion models. Figure 9 shows a sample result of a computation simulation of the discrete model in a 2-dimensional domain. The individual cancer cells are secreting degrading enzymes and proliferating and migrating into the space created (through diffusion and haptotaxis). As can be seen from the figure, because of the stochastic nature of the discrete model individual cancer cells possess mathematically the ability to penetrate the normal tissue at a greater depth than would be predicted usual a deterministic PDE model.

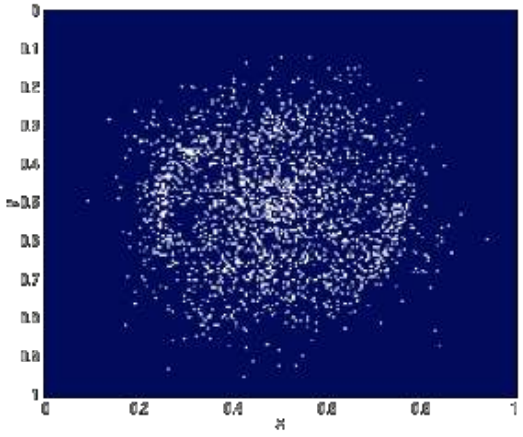

Figure 9. Specimen simulation result from the discrete invasion model of Anderson et al. [25]**.** The figure shows that individual cancer cells can penetrate the normal tissue at great depth. (permission pending)

Other discrete models of invasion have subsequently been developed using a variety of techniques such as the Potts Model [32,33], cellular automata and agent-based models [34-36], hybrid continuum-discrete approaches [26,37] and individual, force-based models [38,39]. One advantage discrete models have over continuum models, is that events at the level of single cells can be considered. Using discrete models, important events such as mutations can be taken into account as well as different phenotypic properties. The introduction of discrete models have also led to the development of so-called "multiscale models", where intracellular events can be modeled using systems of ordinary differential equations and these can then be linked to cellular level parameters [35,38].

Hybrid continuum-discrete models have also been developed over the past 15 years or so to model another very important event in solid tumor growth and development – that of (tumor-induced) angiogenesis. The seminal paper of Anderson and Chaplain [38] initially considered a system of PDEs describing the spatio-temporal interactions of (tip) endothelial cells, n, extracellular matrix (represented by fibronectin), v and tumor angiogenic factor (TAF), a, as follows:

$$\frac{\partial n}{\partial t} = \overbrace{D_n \nabla^2 n}^{\text{random walk}} - \overbrace{\nabla \cdot \left(\chi(a) n \nabla a \right)}^{\text{chemotaxis}} - \overbrace{\nabla \cdot \left(\rho n \nabla v \right)}^{\text{haptotaxis}}$$

$$\frac{\partial v}{\partial t} = \overbrace{\beta n}^{\text{production}} - \overbrace{\gamma n v}^{\text{uptake}}$$

$$\frac{\partial a}{\partial t} = -\overbrace{\eta n a}^{\text{uptake}}.$$

The endothelial cells perform a random walk as well as directed migration via chemotaxis in response to TAF gradients (e.g. VEGF) and haptotaxis, which is directed

migration in response to fibronectin gradients in the extracellular matrix [40,41]. The computational simulation results from the discrete version of the model that incorporated cellular-automata-like rules, such as capillary branching and anastomosis were able to reproduce branched, connected capillaries networks as observed in experimental papers (c.f. [42,43]), as can be seen from Figure 10.

Such discrete models have now been developed to include the effects of blood flow within the capillaries and there currently exist several complementary models in the literature focusing on various aspects of tumor-induced angiogenesis and vascular tumor growth [42-51].

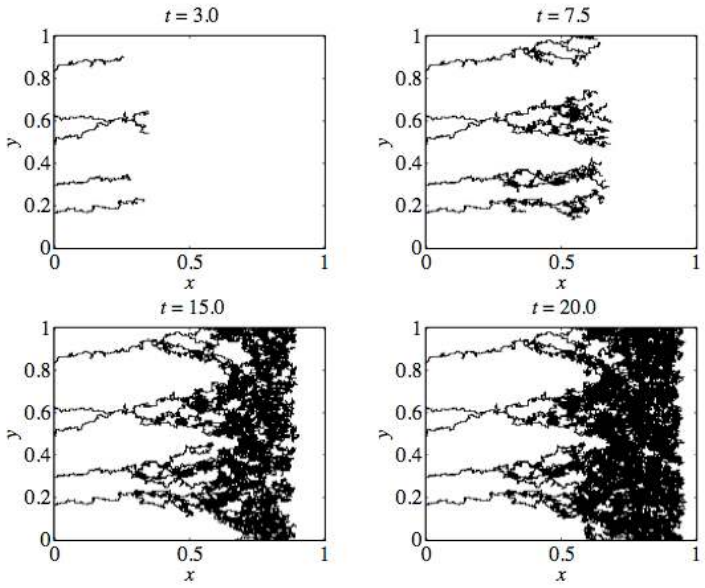

Figure 10. Specimen simulation result from the discrete angiogenesis model of Anderson and Chaplain [52]**.** Individual capillaries (emanating from a parent vessel located on the left-hand vertical axis) respond chemotactically and haptotactically to gradients of TAF and fibronectin to form a branched, connected capillary network that

can connect with the solid tumor (located along the right-hand vertical axis). (permission pending)

Additionally, these discrete angiogenesis models have been adapted and developed to model other systems where the development of blood vessels plays a critical role, such as wound healing [53,54] and retinal development [55].

Discussion

An increasing variety of mathematical models have made their way into cancer research over the past couple of decades. Herein we have illustrated how simple quantitative models are developed and compared with experimental data, and showed how they can be used to simulate complex biological processes and interactions. We have chosen seminal papers as examples, and for simplicity have had to leave out a large body of excellent mathematical modeling literature. The interested reader is referred to recent review articles and books that give a more inclusive overview of the state-of-the-art in cancer modeling [56-59].

Acknowledgements

HE gratefully acknowledges the support of the National Cancer Institute under Award Number U54CA149233 (to Lynn Hlatky). MAJC gratefully acknowledges the support of the ERC Advanced Investigator Grant no. 227619, 'M5CGS—From Mutations to Metastases: Multiscale Mathematical Modelling of Cancer Growth and Spread'.

References

1. Wang CH, Rockhill JK, Mrugala M, Peacock DL, Lai A, Jusenius K, et al. Prognostic significance of growth kinetics in newly diagnosed glioblastomas revealed by combining serial imaging with a novel biomathematical model. Cancer Research. 2009 Dec 1;69(23):9133–40.

2. Macklin P, Edgerton ME, Thompson AM, Cristini V. Patient-calibrated agent-based modelling of ductal carcinoma in situ (DCIS): from microscopic measurements to macroscopic predictions of clinical progression. Journal of Theoretical Biology. 2012 May 21;301:122–40.

3. Gao X, McDonald JT, Hlatky L, Enderling H. Acute and fractionated irradiation differentially modulate glioma stem cell division kinetics. Cancer Research. 2013 Mar 1;73(5):1481–90.

4. Rockne R, Rockhill JK, Mrugala M, Spence AM, Kalet I, Hendrickson K, et al. Predicting the efficacy of radiotherapy in individual glioblastoma patients in vivo: a mathematical modeling approach. Phys. Med. Biol. 2010 Jun 21;55(12):3271–85.

5. Enderling H, Chaplain MAJ, Anderson ARA, Vaidya JS. A mathematical model of breast cancer development, local treatment and recurrence. Journal of Theoretical Biology. 2007 May 21;246(2):245–59.

6. Cappuccio A. Cancer immunotherapy by interleukin-21: potential treatment strategies evaluated in a mathematical model. Cancer Research. 2006 Jul 15;66(14):7293–300.

7. Marcu L, Bezak E. Radiobiological modeling of interplay between accelerated repopulation and altered fractionation schedules in head and neck cancer. J Med Phys. 2009;34(4):206.

8. Powathil GG, Gordon KE, Hill LA, Chaplain MAJ. Modelling the effects of cell-cycle heterogeneity on the response of a solid tumour to chemotherapy Biological insights from a hybrid multiscale cellular automaton model. Journal of Theoretical Biology. Elsevier; 2012 Sep 7;308(C):1–19.

9. Holmgren L, O'Reilly MS, Folkman J. Dormancy of micrometastases: Balanced proliferation and apoptosis in the presence of angiogenesis suppression. Nature Medicine. 1995 Feb;1(2):149–53.

10. Enderling H. Cancer Stem Cells and Tumor Dormancy. Advances in Experimental Medicine and Biology. New York, NY: Springer New York; 2012. pp. 55–71.

11. Skehan P. On the normality of growth dynamics of neoplasms in vivo: a data base analysis. Growth. 1986;50(4):496–515.

12. Prehn RT. The inhibition of tumor growth by tumor mass. Cancer Research. 1991 Jan 1;51(1):2–4.

13. Hart D, Shochat E, Agur Z. The growth law of primary breast cancer as inferred from mammography screening trials data. Br J Cancer. 1998 Aug;78(3):382–7.

14. Norton L. Cancer stem cells, self-seeding, and decremented exponential growth: theoretical and clinical implications. Breast Dis. IOS Press; 2008;29(1):27–36.

15. Sachs RK, Hlatky LR, Hahnfeldt P. Simple ODE models of tumor growth and anti-angiogenic or radiation treatment. Mathematical and Computer Modelling. Elsevier; 2001;33(12):1297–305.

16. McAneney H, O'Rourke SFC. Investigation of various growth mechanisms of solid tumour growth within the linear-quadratic model for radiotherapy. Phys. Med. Biol. 2007 Jan 23;52(4):1039–54.

17. Gompertz B. On the nature of the function expressive of the law of human mortality, and on a new mode of determining the value of life contingencies. Philosophical transactions of the Royal Society of London. 1825;115:513–83.

18. Winsor CP. The Gompertz curve as a growth curve. Proc. Natl. Acad. Sci. U.S.A. 1932 Jan 5;18(1):1–8.

19. Spratt JS, Meyer JS, Spratt JA. Rates of growth of human solid neoplasms: Part I. J Surg Oncol. 1995 Oct;60(2):137–46.

20. Spratt JS, Meyer JS, Spratt JA. Rates of growth of human neoplasms: Part II. J Surg Oncol. 1996 Jan;61(1):68–83.

21. Hahnfeldt P, Panigrahy D, Folkman J, Hlatky L. Tumor development under angiogenic signaling: a dynamical theory of tumor growth, treatment response, and postvascular dormancy. Cancer Research. 1999 Oct 1;59(19):4770–5.

22. Gatenby RA, Gawlinski ET. A reaction-diffusion model of cancer invasion. Cancer Research. 1996 Dec 15;56(24):5745–53.

23. Gatenby RA. The potential role of transformation-induced metabolic changes in tumor-host interaction. Cancer Research. 1995 Sep 15;55(18):4151–6.

24. Perumpanani AJ, Sherratt JA, Norbury J, Byrne HM. Biological inferences from a mathematical model for malignant invasion. Invasion Metastasis. 1996;16(4-5):209–21.

25. Anderson ARA, Chaplain MAJ, Newman EL, Steele RJC, Thompson AM. Mathematical modelling of tumour invasion and metastasis. Computational and Mathematical Methods in Medicine. 2000;2(2):129–54.

26. Anderson ARA. A hybrid mathematical model of solid tumour invasion: the importance of cell adhesion. Mathematical Medicine and Biology. 2005 Mar 18;22(2):163–86.

27. Chaplain MAJ, Lolas G. Mathematical modelling of cancer cell invasion of tissue: the role of the urokinase plasminogen activation system. Math. Models Methods Appl. Sci. 2005 Nov;15(11):1685–734.

28. Andasari V, Gerisch A, Lolas G, South AP, Chaplain MAJ. Mathematical modeling of cancer cell invasion of tissue: biological insight from mathematical analysis and computational simulation. J. Math. Biol. 2010 Sep 26;63(1):141–71.

29. Frieboes HB. An integrated computational/experimental model of tumor invasion. Cancer Research. 2006 Feb 1;66(3):1597–604.

30. Gerisch A, Chaplain MAJ. Mathematical modelling of cancer cell invasion of tissue: Local and non-local models and the effect of adhesion. Journal of Theoretical Biology. 2008 Feb;250(4):684–704.

31. Chaplain MAJ, Ganesh M, Graham IG. Spatio-temporal pattern formation on spherical surfaces: numerical simulation and application to solid tumour growth. J. Math. Biol. Springer-Verlag; 2001 May 1;42(5):387–423.

32. Turner S, Sherratt JA. Intercellular adhesion and cancer invasion: a discrete simulation using the extended Potts model. Journal of Theoretical Biology. 2002 May 7;216(1):85–100.

33. Popławski NJ, Agero U, Gens JS, Swat M, Glazier JA, Anderson ARA. Front instabilities and invasiveness of simulated avascular tumors. Bull Math Biol. 2009 Feb 21;71(5):1189–227.

34. Kansal AR, Torquato S, Harsh GR IV, Chiocca EA, Deisboeck TS. Cellular automaton of idealized brain tumor growth dynamics. BioSystems. 2000 Feb;55(1-3):119–27.

35. Zhang L, Wang Z, Sagotsky JA, Deisboeck TS. Multiscale agent-based cancer modeling. J. Math. Biol. 2008 Sep 12;58(4-5):545–59.

36. Enderling H, Anderson ARA, Chaplain MAJ, Beheshti A, Hlatky L, Hahnfeldt P. Paradoxical dependencies of tumor dormancy and progression on basic cell kinetics. Cancer Research. 2009 Nov 11;69(22):8814–21.

37. Rejniak KA, Anderson ARA. Hybrid models of tumor growth. WIREs Syst Biol Med. 2010 Jul 7;3(1):115–25.

38. Ramis-Conde I, Chaplain MAJ, Anderson ARA. Mathematical modelling of cancer cell invasion of tissue. Mathematical and Computer Modelling. 2008 Mar;47(5-6):533–45.

39. Ramis-Conde I, Drasdo D, Anderson ARA, Chaplain MAJ. Modeling the Influence of the E-Cadherin-β-Catenin Pathway in Cancer Cell Invasion: A Multiscale Approach. Biophysical Journal. 2008 Jul;95(1):155–65.

40. McCarthy JB, Palm SL, Furcht LT. Migration by haptotaxis of a Schwann cell tumor line to the basement membrane glycoprotein laminin. The Journal of Cell Biology. 1983 Sep;97(3):772–7.

41. Davis JM, John JS, Cheung HT. Haptotactic activity of fibronectin on lymphocyte migration in vitro. Cellular Immunology. 1990 Aug;129(1):67–79.

42. Macklin P, McDougall S, Anderson ARA, Chaplain MAJ, Cristini V, Lowengrub J. Multiscale modelling and nonlinear simulation of vascular tumour growth. J. Math. Biol. 2008 Sep 10;58(4-5):765–98.

43. McDougall SR, Anderson ARA, Chaplain MAJ. Mathematical modelling of dynamic adaptive tumour-induced angiogenesis: Clinical implications and therapeutic targeting strategies. Journal of Theoretical Biology. 2006 Aug;241(3):564–89.

44. Alarcón T, Owen MR, Byrne HM, Maini PK. Multiscale modelling of tumour growth and therapy: the influence of vessel normalisation on chemotherapy. Computational and Mathematical Methods in Medicine. 2006;7(2-3):85–119.

45. Bauer AL, Jackson TL, Jiang Y. A cell-based model exhibiting branching and anastomosis during tumor-induced angiogenesis. Biophysical Journal. Elsevier; 2007 May 1;92(9):3105–21.

46. Jackson T, Zheng X. A cell-based model of endothelial cell migration, proliferation and maturation during corneal angiogenesis. Bull Math Biol. 2010 Jan 6;72(4):830–68.

47. Owen MR, Alarcón T, Maini PK, Byrne HM. Angiogenesis and vascular remodelling in normal and cancerous tissues. J. Math. Biol. 2008 Oct 22;58(4-5):689–721.

48. Szczerba D, Kurz H, Szekely G. A computational model of intussusceptive microvascular growth and remodeling. Journal of Theoretical Biology. Elsevier; 2009 Dec 21;261(4):570–83.

49. Bentley K, Gerhardt H, Bates PA. Agent-based simulation of notch-mediated tip cell selection in angiogenic sprout initialisation. Journal of Theoretical Biology. 2008 Jan;250(1):25–36.

50. Welter M, Bartha K, Rieger H. Vascular remodelling of an arterio-venous blood vessel network during solid tumour growth. Journal of Theoretical Biology. 2009 Aug;259(3):405–22.

51. Wu J, Long Q, Xu S, Padhani AR. Study of tumor blood perfusion and its variation due to vascular normalization by anti-angiogenic therapy based on 3D angiogenic microvasculature. Journal of Biomechanics. 2009 Apr;42(6):712–21.

52. Anderson AR, Chaplain MA. Continuous and discrete mathematical models of tumor-induced angiogenesis. Bull Math Biol. 1998 Sep;60(5):857–99.

53. McDougall S, Dallon J, Sherratt J, Maini P. Fibroblast migration and collagen deposition during dermal wound healing: mathematical modelling and clinical implications. Philosophical Transactions of the Royal Society A: Mathematical, Physical and Engineering Sciences. 2006 Jun 15;364(1843):1385–405.

54. Machado CB, de Albuquerque Pereira WC, Talmant M, Padilla F, Laugier P. Computational evaluation of the compositional factors in fracture healing affecting ultrasound axial transmission measurements. Ultrasound in Medicine & Biology. Elsevier Ltd; 2010 Aug 1;36(8):1314–26.

55. Watson MG, McDougall SR, Chaplain MAJ, Devlin AH, Mitchell CA. Dynamics of angiogenesis during murine retinal development: a coupled in vivo and in silico study. Journal of The Royal Society Interface. 2012 Jul 25;9(74):2351–64.

56. Araujo R. A history of the study of solid tumour growth: the contribution of mathematical modelling. Bull Math Biol. 2004 Sep;66(5):1039–91.

57. Anderson ARA, Chaplain MAJ, Rejniak KA, Fozard JA. Single-cell-based models in biology and medicine. Mathematical Medicine and Biology. 2008 May 25;25(2):185–6.

58. Lowengrub JS, Frieboes HB, Jin F, Chuang Y-L, Li X, Macklin P, et al. Nonlinear modelling of cancer: bridging the gap between cells and tumours. Nonlinearity. 2009 Dec 17;23(1):R1–R91.

59. Deisboeck TS, Stamatakos GS. Multiscale cancer modeling. CRC Press; 2011.